THE STRUCTURE OF AMORPHOUS SOLIDS

W. RULAND

Union Carbide European Research Associates, S.A., Brussels 18, *Belgium*

INTRODUCTION

Before the discovery of x-ray diffraction it was relatively easy to make definite statements about 'crystalline' and 'amorphous': if the outer contours of a material showed crystal faces it was considered to be crystalline, a material showing irregular contours without faces was considered amorphous. In fact, such a definition makes proper use of the word 'amorphous', the etymological meaning of which is 'without form' and not 'disordered structure'. After the discovery of x-ray diffraction many of the substances considered as amorphous turned out to be micro-crystalline and, since the internal structure is by far more essential for the understanding of the solid state than the outer contours, the word 'amorphous' was more and more used in the sense 'disordered structure' or 'frozen-in liquid structure' which means that an amorphous structure is considered essentially 'non-crystalline' and with some resemblance to the structure of liquids. It was especially the latter aspect which was pursued in the earlier studies of the glass structure[1, 2] and in the interpretation of rubber elasticity[3–6].

The most general statement one can make about the difference between 'crystalline' and 'amorphous' is that the former implies a three-dimensional long-range order whereas the latter does not. Since intermediate structures with one-dimensional or two-dimensional long-range order exist (e.g. in liquid crystals) and the term 'amorphous' is in general not used for such structures, it is more appropriate to use the term 'non-crystalline' for all structures which do not possess a three-dimensional long-range order and reserve the term 'amorphous' for those structures which do not have a long-range order in any direction.

General agreement exists as far as the absence of long-range order is concerned; however, there is a definite disagreement about the basic feature of the short-range order in liquid and liquid-like structures. One school, of which the main protagonist is Bernal[7], postulates that this short-range order bears no resemblance whatsoever to the crystalline order whereas the other, of which the principal advocate is Hosemann[8], considers a 'paracrystalline' structure as representative for all types of short-range order. The attraction of the 'paracrystalline' concept is its relatively concise theory which greatly facilitates the interpretation of scattering diagrams, whereas the Bernal model does not lend itself easily to a straightforward mathematical treatment so that a quantitative check of its validity by scattering experiments is extremely difficult.

It is not the aim of this paper to review the earlier work done in this field, for which one finds an excellent bibliography by Kruh[9], but to discuss some

problems which are related to the non-crystalline state of macromolecular substances.

THEORETICAL

General

Any interpretation of the scattering from a non-crystalline solid can be derived from the basic equation of the kinematic scattering theory

$$I(\vec{s}) = \mathfrak{F}[\rho^{*2}(\vec{r})]$$

where $$\mathfrak{F} = \int_v \exp(2\pi i \vec{r}\vec{s})\mathrm{d}v$$

and

$$\rho^{*2} = \int_v \rho(\vec{y})\,\rho(\vec{r}+\vec{y})\mathrm{d}v_y$$

I is the corrected coherent scattering intensity in electron units,

$\vec{s}$ is the reciprocal space vector ($s = 2\sin\theta/\lambda$),

$\vec{r}$ the position vector in physical space,

$\rho(\vec{r})$ the distribution of electron density, and

$\vec{y}$ an auxiliary variable in physical space.

ρ^{*2} is called the auto-correlation function or the self-convolution of ρ and is related to but not identical with the Patterson function used in crystal structure analysis.

Taking into account that the scattering of the total irradiated volume (near $s = 0$) is, in general, not measurable, one has to replace ρ by $(\rho - \langle\rho\rangle_v)$ if I is to be the observable intensity ($\langle\rho\rangle_v$ is the volume average of ρ).

The usual procedure for non-crystalline substances is to consider I as independent of the direction of $\vec{s}$ which means that ρ is independent of the direction of $\vec{r}$, and one then obtains

$$I(s) = 4\pi\int_0^\infty r^2\rho^{*2}(r)\,\frac{\sin 2\pi rs}{2\pi rs}\,\mathrm{d}r$$

from which follows[10]

$$sI(s) = 2\int_0^\infty r\rho^{*2}(r)\sin 2\pi rs\,\mathrm{d}r$$

$$r\rho^{*2}(r) = 2\int_0^\infty sI(s)\sin 2\pi rs\,\mathrm{d}s$$

To obtain more detail, $\rho^{*2}(r)$ is generally 'sharpened' by using $(I - \sum_i f_i^2)/\sum_i f_i^2$ instead of I in the transform, and errors due to the truncation of I are minimized by a suitable 'modification function'[11]. The result is called 'radial atomic distribution function'. A full discussion of the significance of parameters derived from this function as well as a critical survey of its limitations although worthwhile would exceed the scope of this paper. One can, however, state that an extreme accuracy of the intensity measurements

and of the corrections for the intensity is required in order to obtain results which are worth interpreting in detail. The older work in this field cannot be expected to possess this accuracy since the experimental possibilities were rather limited and the scattering functions used for the computation of the corrections (coherent and incoherent atomic scattering) were based on relatively crude approximations. The progress made in recent years in both the theory and the experimental techniques justifies a revision of the essential part of the older work. Encouraging examples of recent work in this field are the studies on liquid metals by Kaplow, Strong and Averbach[12]; Fessler, Kaplow and Averbach[13]; Kaplow, Rowe and Averbach[14] and Hosemann and Lemm[15], which show that radial atomic distribution functions can be interpreted quantitatively up to high values of r in terms of a short-range order which has preserved a memory of the arrangement of the atoms in the crystal state. It has become more and more accepted to call such a short-range order 'paracrystalline' even when it does not correspond to the exact mathematical definition of the coordination statistics as proposed by Hosemann. In a way, this more qualitative definition is similar to the old 'cybotactic' model of Stewart[16].

An important consequence of such a model is that it necessarily implies a finite size of the 'paracrystallites' and thus the existence of some sort of boundary region between them. Such a grainy structure seems, at first sight, to be in contradiction with the basically isotropic and homogeneous structure of a liquid, but the isotropy and the homogeneity of such a structure are properties which are verified only on a relatively large scale in space and time. In fact, a relatively densely packed system of particles can be considered homogeneous and isotropic only above a certain limit in space, and the isotropy of ρ^{*2} implies no information on the isotropy of ρ on a scale smaller than the size of the irradiated volume.

If the scattering of various monatomic liquids can be interpreted consistently by a 'paracrystalline' model, there is even more justification for the use of such a model for the short-range order of particles with strongly anisotropic shapes since a dense packing of such particles is not possible without a certain correlation between the position and the orientation of the particles relative to each other. In fact, there are a number of indications [17–22] that the short-range order in amorphous macromolecular substances is anisotropic (the axes of neighbouring chains have a tendency to be parallel), that a grain structure exists in such substances and that the grains show the properties of uni-axial paracrystallites. The only essential difference between the structure of these substances and the nematic phase of liquid crystals seems to be the size of the anisotropic domains.

A quantitative study of the scattering of such substances should, in principle, give information on the size and the disorder parameters of these domains. In order to give an idea of the general features to be expected we shall discuss two idealized cases, a bundle of linear molecules and a stack of planar molecules without further positional correlation than the parallelism of the principal axes.

Anisotropic short-range order

A practical way to treat such a problem is to consider first the three-dimen-

sional auto-correlation function in the physical space and the corresponding intensity distribution in reciprocal space, and to perform the spherical averaging in both spaces afterwards.

In both cases we can define the auto-correlation function ρ_D of a domain by

$$\rho_D^{*2} = N_M \langle \rho_M^{*2} \rangle_\psi + \langle \rho_M \rangle_\psi^{*2} * (z^{*2} - N_M \delta)$$

where N_M is the number of molecules in the domain, ρ_M is the electron density distribution of the molecule with respect to its centre and the principal axis, $\langle \rangle_\psi$ the average about this axis (ψ being the azimuth in the plane perpendicular to this axis), δ is the Dirac delta distribution and z the distribution of the centres of the molecules in space.

Neglecting the effect of finite domain size and inter-domain correlations, the radial distribution function of the ensemble of domains can be expressed as

$$\rho^{*2} = N_D \langle \rho_D^{*2} \rangle_\omega$$

where N_D is the number of the domains and $\langle \rangle_\omega$ the average over the solid angle ω (spherical average). The spherical averaging of $\rho_D{}^{*2}$ can be performed in two steps, first averaging over ψ and then over the colatitude φ, which gives

$$\langle \rho_D^{*2} \rangle_\omega = \int_0^{\pi/2} \langle \rho_D{}^{*2} \rangle_\psi \sin\varphi \, d\varphi$$

and

$$\langle \rho_D^{*2} \rangle_\psi = N_M \langle \rho_M{}^{*2} \rangle_\psi + \langle \rho_M \rangle_\psi{}^{*2} * (\langle z^{*2} \rangle_\psi - N_M \delta)$$

The corresponding expressions for the scattering intensity are

$$\langle I_D \rangle_\psi = N_M \langle | F^2 | \rangle_\psi + | \langle F \rangle_\psi{}^2 | \cdot (\langle | \mathcal{Z}^2 | \rangle_\psi - N_M)$$

and

$$I(s) = N_D \cdot \int_0^{\pi/2} \langle I_D \rangle_\psi \sin\varphi \, d\varphi.$$

Performing the spherical averaging only on the first term on the right-hand side in the equation for $\langle I_D \rangle_\psi$ one obtains

$$I(s) = N \cdot \langle | F^2 | \rangle_\omega$$

$$= N \cdot \sum_j \sum_k f_j f_k \frac{\sin 2\pi r_j k s}{2\pi r_j k s}$$

the well-known Debye equation for the scattering of a molecular gas ($N = N_D \cdot N_M$ is the total number of molecules). The second term contains the intermolecular interferences (a similar expression has been given by Guinier and Fournet[23]).

Figure 1 shows the function $\langle \rho^{*2}{}_D \rangle_\psi$ for a bundle of linear molecules. For simplicity, the molecule is represented only by the centres of the repeat units and the packing in the bundle is taken to be hexagonal close-packed. As would be expected, the intramolecular distances appear sharply, whereas the intermolecular distances are represented by broad streaks parallel to the principal axis. Since $\langle \rho_D^{*2} \rangle_\psi$ has cylindrical symmetry, these streaks represent the sections of hollow cylinders. The spherical average of such distributions (*Figure 2*) produces asymmetric peaks with the maximum

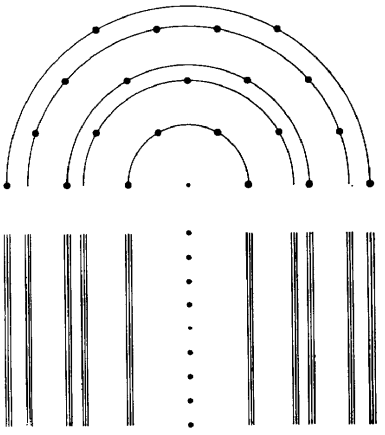

Figure 1. Auto-correlation function for a bundle of linear molecules (schematic).

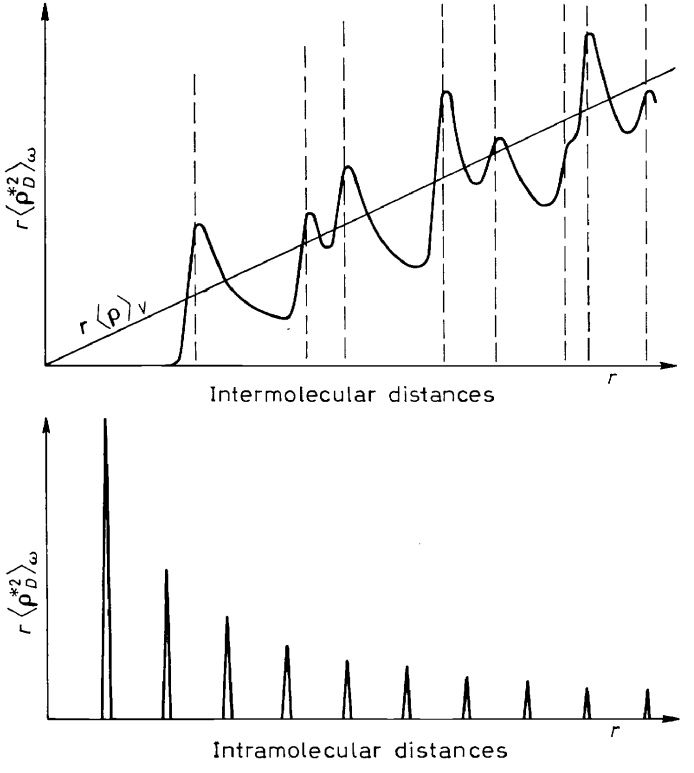

Figure 2. Components of the radial distribution function for a bundle of linear molecules (schematic).

shifted to higher values of r. The profile of these peaks is related to the cross-section of the wall of the cylinder in the same way as the profile of a random-layer line is related to an (hk) interference[24–27].

Figure 3 shows the corresponding intensity distribution in reciprocal space. It is now the effect of the intermolecular distances which appears sharply, whereas the intramolecular interferences form streaks perpendicular to the principal axis. These streaks are sections of planes, the spherical averages of which appear as step-functions in the radial intensity distribution (*Figure 4*) when plotted as $sI(s)$ versus s.

Figure 5 shows the auto-correlation function for a stack of planar molecules. The intermolecular distances form a series of planes perpendicular to the principal axis; the intramolecular distances appear sharply. The pattern is similar to that of the intensity distribution for a bundle of linear molecules and thus shows similar features in the spherical average (*Figure 6*). The corresponding intensity distribution (*Figure 7*) shows a series of hollow cylinders which represent the intramolecular interferences, and a series of equidistant points which stem from the parallel stacking. The radial intensity distribution (*Figure 8*) shows asymmetrical intramolecular interferences and symmetrical intermolecular interferences.

From this, one can conclude that information on the molecular structure is more directly accessible in the radial distribution function, whereas the intensity distributions give a clearer picture of the intermolecular arrangement. It is, however, possible to obtain the desired information also from the asymmetrical peaks. In the case of the spherical average of planes with finite thickness (*Figures 4* and *6*) the profile of the cross-section of the planes produces step-functions with smoothed edges in $sI(s)$. This can be considered as a convolution of the profile of the cross-section with an ideally sharp step-function from which the profile can be obtained by taking the first derivative. In the case of asymmetrical peaks produced by the spherical average of rods or cylinders, the profile of the cross-section can be obtained by a Fourier transform method[27].

The profile of the symmetrical peaks in the radial distributions can be considered as a linear projection of the three-dimensional distributions as long as their width is sufficiently small compared with the distance of the centre of the peak from the origin of the space in question. This so-called 'tangent plane approximation' is generally used for the interpretation of powder diagrams. In the case of amorphous substances this approximation is not always valid since the peaks can have considerable broadening. This problem has been discussed in detail by Townsend[28] and a Fourier transform method for computing the true spherical average for peaks which are laterally broadened by crystallite size effects only has been given by Warren and Bodenstein[29]. A simple solution of this problem has been given by Ruland[30] for a spherically broadened peak in which case one can show that the profile in $sI(s)$ corresponds to the linear projection (*Figure 9*). It can be shown that, for the same reasons, the broadening due to truncation effects is symmetrical only in $r\langle\rho^{*2}\rangle_\omega$. This indicates that the direct study of the functions $r\langle\rho^{*2}\rangle_\omega$ and $sI(s)$ is, in certain cases, preferable to a study of $\langle\rho^{*2}\rangle_\omega$ and $I(s)$, or $r^2\langle\rho^{*2}\rangle_\omega$ and $s^2I(s)$, respectively.

So far we have neglected the effect of finite domain size and inter-domain

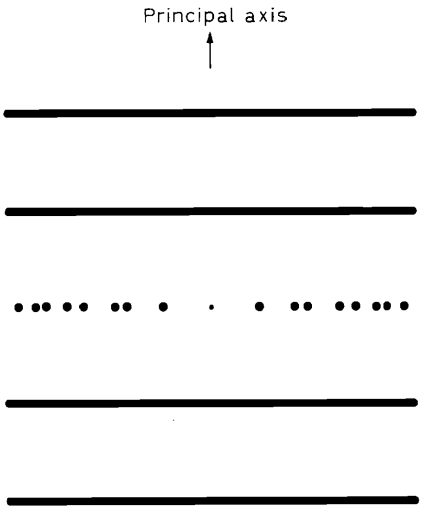

Figure 3. Intensity distribution in reciprocal space for a bundle of linear molecules (schematic).

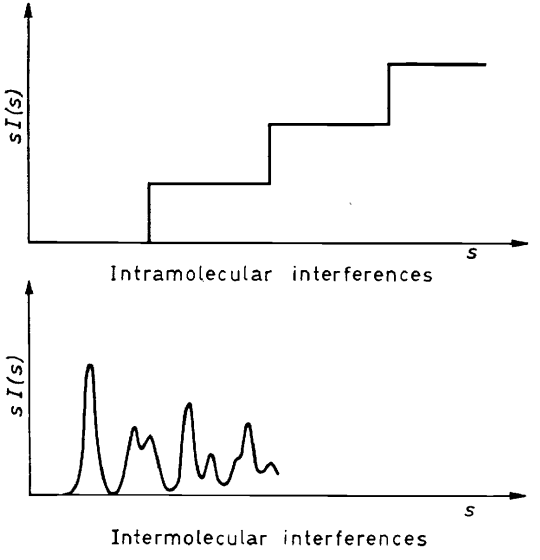

Figure 4. Components of the radial intensity distribution for a bundle of linear molecules (schematic).

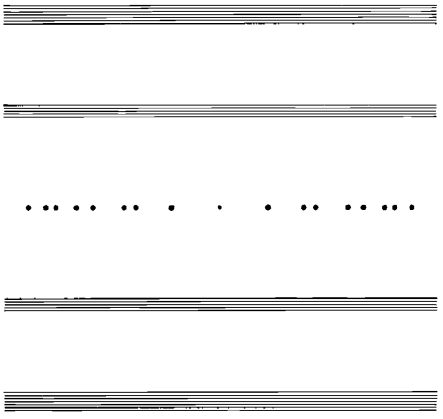

Figure 5. Auto-correlation function for a stack of planar molecules (schematic).

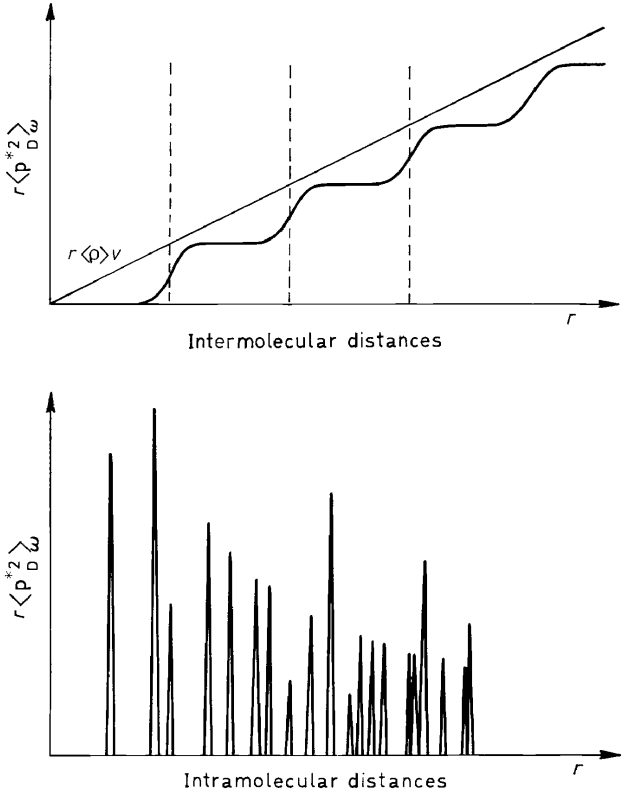

Figure 6. Components of the radial distribution function for a stack of planar molecules (schematic).

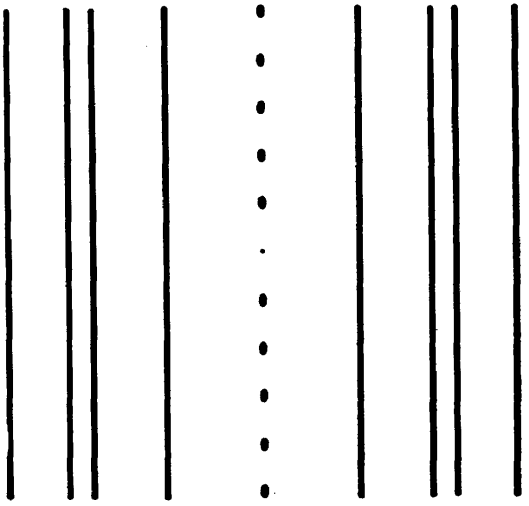

Figure 7. Intensity distribution in reciprocal space for a stack of planar molecules (schematic).

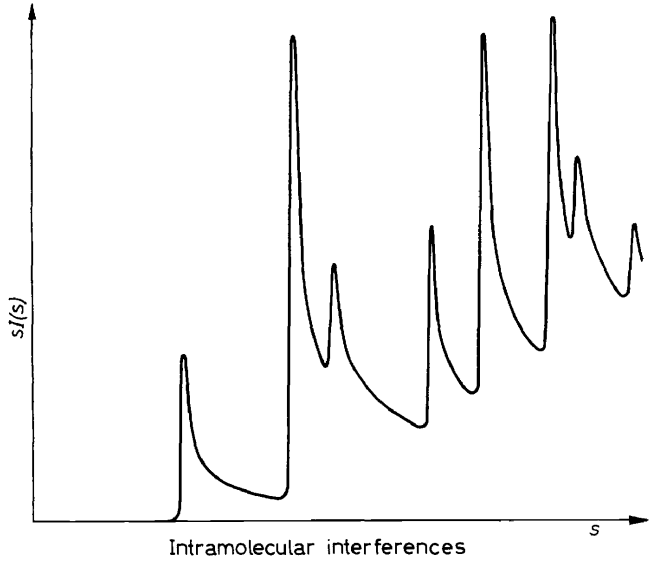

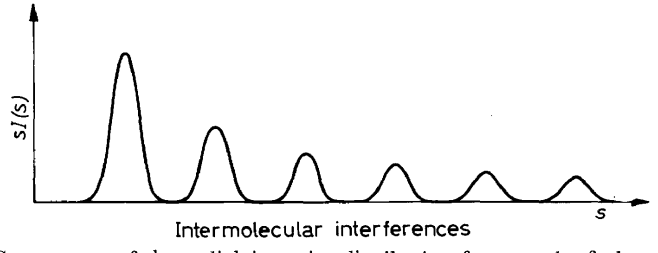

Figure 8. Components of the radial intensity distribution for a stack of planar molecules (schematic).

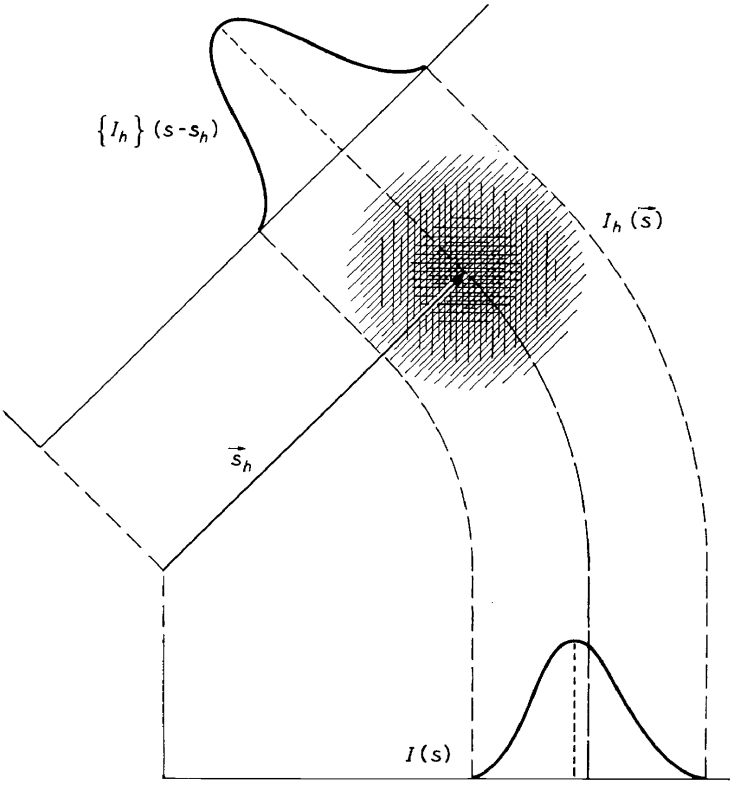

Figure 9. Spherical average and linear projection of a spherically broadened peak (By the courtesy of *Carbon*).

correlations in order to make the similarities between radial distribution functions and intensity distributions more evident. If one assumes a sufficient disorder in the distribution of the centres of the domains and their mutual orientation one can write the approximation

$$\rho^{*2} = \mathcal{N}_D \langle \rho_D^{*2} \rangle_\omega + \langle \rho \rangle_v^2 (\Upsilon_v^{*2} - \mathcal{N}_D \Upsilon_D^{*2})$$

where $\langle \rho \rangle_v$ is the volume average of the electron density, Υ_v is the shape function of the irradiated volume and Υ_D the shape function of the average space occupied by a domain. (A shape function has the value unity inside the boundaries of a body and the value zero outside of the boundaries). Since ρ^{*2} is not directly observable but only $(\rho - \langle \rho \rangle_v)^{*2}$ this gives

$$(\rho - \langle \rho \rangle_v)^{*2} = \mathcal{N}_D (\rho_D^{*2} - \langle \rho \rangle_v^2 \Upsilon_D^{*2})$$

A schematic presentation of such a function is given in *Figure 10* for a stack of planar molecules.

Small-angle scattering

We have so far dealt with the scattering at relatively wide angles where the scattering of a liquid and the scattering of an amorphous solid show

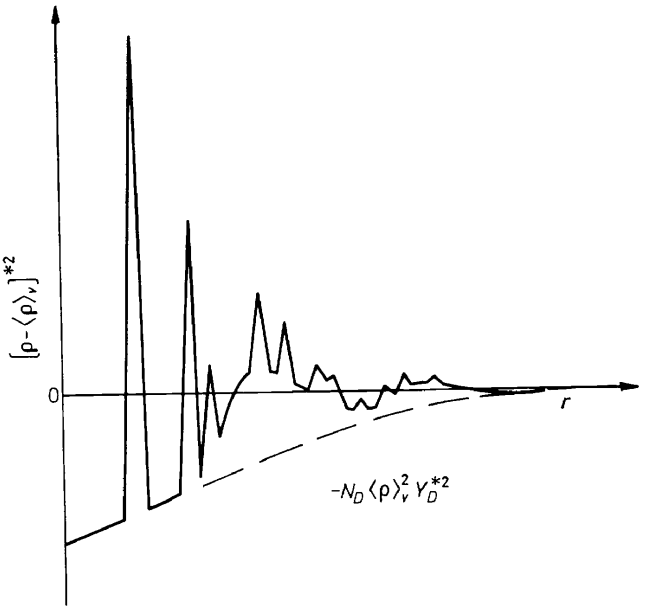

Figure 10. Radial distribution function (schematic) for a stack of planar molecules, taking into account finite domain size and a dense but disordered packing of the domains.

similar features. This is, in general, not the case for the small-angle scattering. The small-angle scattering of a liquid is monotonic since the density fluctuations in a liquid are small and homogeneous, and there is a direct relation between the fluctuation of the particle density and the compressibility. An amorphous solid can show very high density fluctuations which cause various types of small-angle scattering of sometimes considerable intensity, and there is no direct correlation between the density fluctuation and the compressibility. The differences in the magnitude and the type of density fluctuations can be assessed by a weighted average of the observable scattering intensity (I_{obs}) near the origin of the reciprocal space. Starting with

$$I_{\text{obs}} = \mathfrak{F}\,(\Delta\rho)^{*2}$$

where

$$\Delta\rho = \rho - \langle\rho\rangle_v,$$

one finds

$$\int I_{\text{obs}}\,\Phi_S \mathrm{d}v = \int \Delta^{*2}\rho\; Y_S\,\mathrm{d}v$$

where Φ_S is the Fourier transform of Y_S, and Y_S is the shape function of a sampling volume for the averaging. Provided that the sampling volume is small compared with the total irradiated volume the above integrals are equal to

$$V\,V_S\,(\langle\rho^2\rangle_S - \langle\rho\rangle_v^2)$$

where V is the total irradiated volume, V_S the sampling volume and $\langle\rho^2\rangle_S$ the average of the square of the density inside the sampling volume. By proper normalization one obtains from this expression the density fluctuation

$$\frac{\langle\rho^2\rangle_S - \langle\rho\rangle_v^2}{\langle\rho\rangle_v^2}$$

as a function of the sampling volume. For liquids, the density fluctuation as a function of the sampling volume tends rapidly towards a constant value when the dimensions of the sampling volume exceed the range of interparticle interactions. This means that the small-angle scattering intensity of a liquid tends towards a constant value when s approaches zero.

In amorphous materials, the density fluctuations can continue to vary as a function of the sampling volume up to large dimensions, for example, due to the existence of a micropore system. This means that the small-angle scattering does in general not tend towards a constant value as in liquids. However, if the short-range order is similar to that in a liquid, one should expect a constant intensity component from this in addition to the small-angle scattering from other structural features.

In connection with this discussion it should be mentioned that the fluctuations of a two- or three-dimensional paracrystal as defined by Hosemann and Bagchi[8] are a function of the size of the paracrystallite, and tend towards infinity if the size becomes infinite. It can be shown that the spherical average of the small-angle scattering of a finite three-dimensional paracrystal with equal distance statistics along the main axes is given by

$$I(s) = \frac{1}{v_P} \Phi^2{}_P * \left[\frac{3}{2\pi s^2} \frac{\Delta^2 a}{a^2} + \frac{3}{2s} \left(\frac{\Delta^2 a}{a^2} \right)^2 + \left(\frac{\Delta^2 a}{a^2} \right)^3 \right]$$

where Φ_P is the shape factor and v_P the volume of the paracrystal, and $\Delta^2 a/a^2$ the relative mean square deviation along the main axes. An inspection of this equation shows that only the last term between the square brackets yields a constant intensity distribution; the others form a peak with a maximum at $s = 0$, the intensity of which increases with increasing volume of the paracrystal. This feature appears to be due to the basic hypothesis made in Hosemann's theory of the paracrystal that the two- or three-dimensional disorder statistics can be composed of mutually independent one-dimensional statistics along the main axes. A one-dimensional paracrystal, on the contrary, gives a constant intensity at small angles[10] as observed experimentally for liquids. This discrepancy indicates that the application of a multidimensional disorder model as defined by Hosemann for the quantitative evaluation of scattering effects is limited to the interpretation of the wide-angle scattering (interparticle interferences), and that the theory of the multidimensional paracrystal has to be further developed and refined before it can be used for the interpretation of the continuous small-angle scattering due to density fluctuations.

EXPERIMENTAL RESULTS

In this section a short survey will be given of experimental proofs and justifications for the theoretical treatment given in the last section. This survey is incomplete since it is based mainly on the authors' own contributions in the field and, for this reason, the anisotropic short-range order of planar molecules is treated in more detail than that of linear molecules.

Linear molecules

In a study of Nylons of various degrees of crystallinity[31] it was found that the total coherent scattering intensity, when plotted as $sI/\bar{f}^2$ versus s, shows well-defined steps near $s = 0{\cdot}4$ and $s = 0{\cdot}8$ (*Figure 11*). These steps are the intramolecular interferences of portions of extended chain configurations, and the position of the steps corresponds roughly to the average

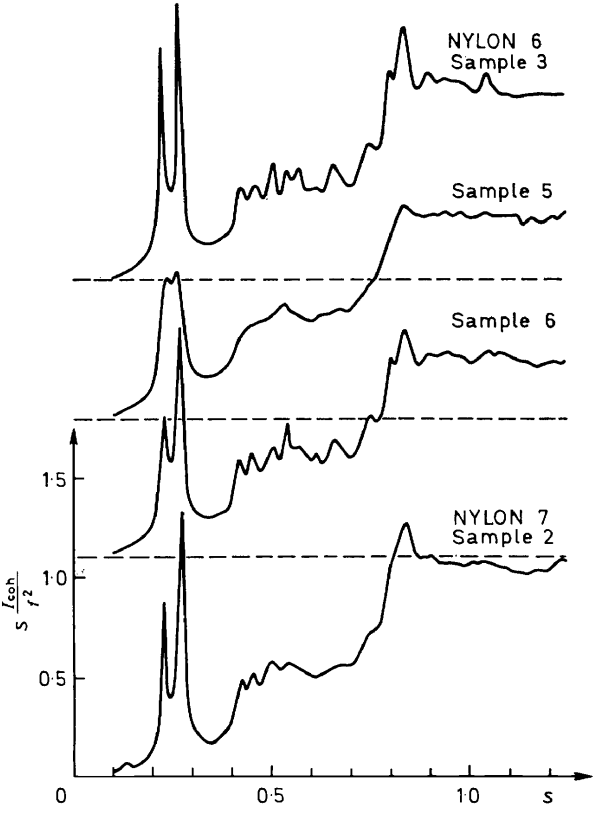

Figure 11. A plot of $sI/\bar{f}^2$ versus s for samples of Nylon 6 and Nylon 7 (By the courtesy of *Polymer*).

repeat distance ($\simeq 2{\cdot}5$ Å) of the zigzag. The most interesting feature is that the step height in the normalized intensity distributions does not show any significant change with crystallinity and corresponds roughly to the theoretical value obtained if one considers the total material to be in the form of portions of extended chain configurations. This means that the majority of the molecules in the amorphous material is also in such a form.

Intensity maps of the diffuse disorder scattering of various Nylons[32] in fibre form show this effect more clearly (*Figures 12, 13* and *14*). The resemblance between these maps and the schematic presentation in *Figure 3* is evident. The modulations on the streaks perpendicular to the fibre axis

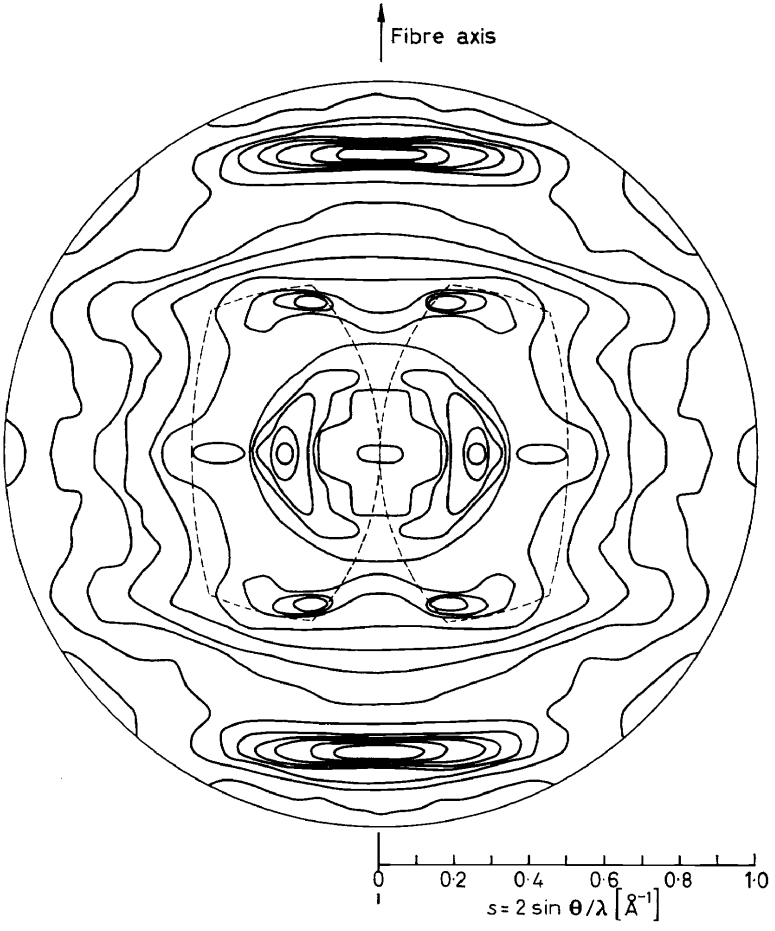

Figure 12. Diffuse disorder scattering of Nylon 6 (By the courtesy of *Norelco Reporter*)

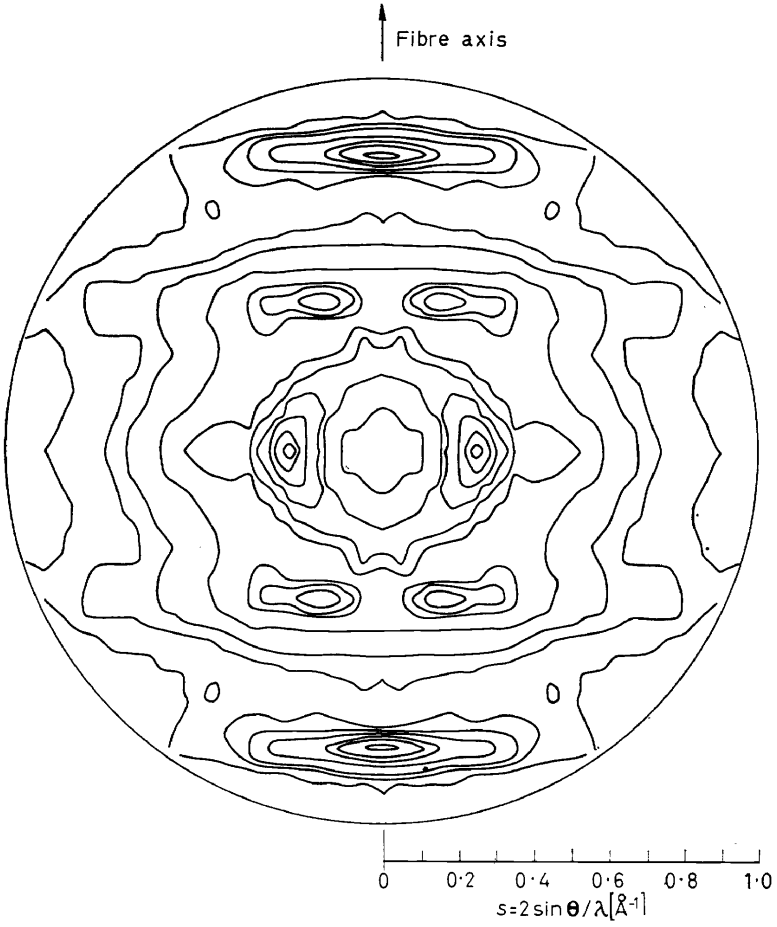

Figure 13. Diffuse disorder scattering of Nylon 66 (By the courtesy of *Norelco Reporter*).

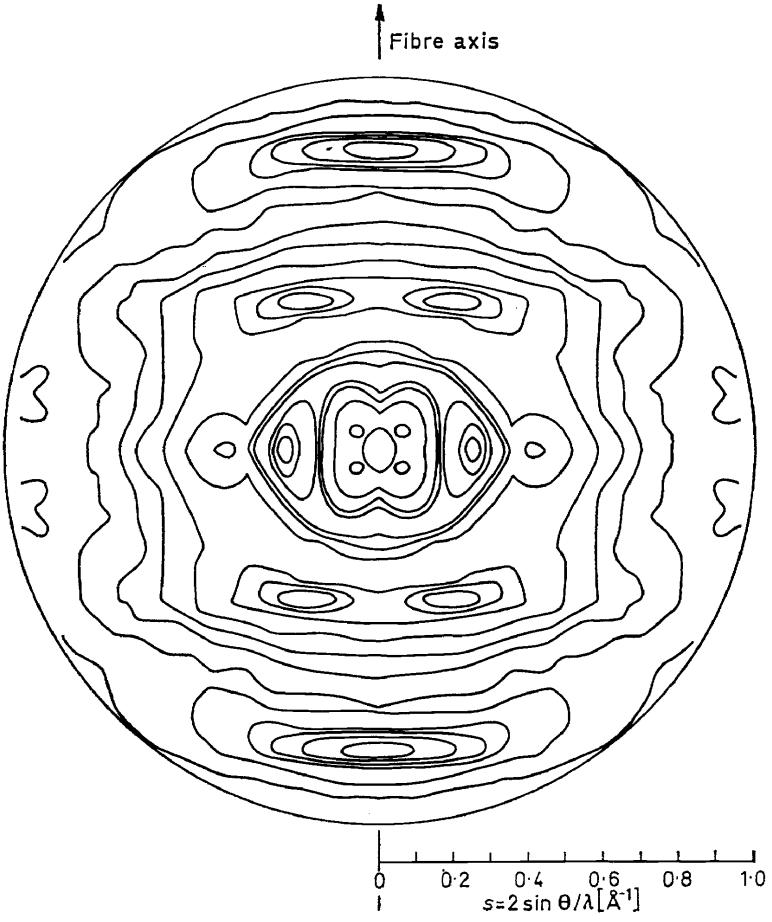

Figure 14. Diffuse disorder scattering of Nylon 11 (By the courtesy of *Norelco Reporter*).

(the intramolecular interferences) are due to the structure factor of the repeat unit of the chain. The diffuse maxima on the meridian are the intermolecular interferences corresponding to bundles of linear molecules. A quantitative evaluation to determine the fraction of the material contributing to these features of the intensity distribution was not carried out, but one can conclude from the absence of any significant isotropic interferences that the anisotropic intensity distribution is representative for the major part of the material, which means that at least some of the amorphous domains are anisotropic and preferentially oriented.

Planar molecules

Radial distribution functions for stacks of planar molecules are shown in *Figure 15*. These functions have been determined in earlier work[33], on the structure of coal. Taking into account the broadening of the intramolecular peaks due to truncation effects, the similarity between *Figure 15* and *Figure 10* becomes evident. True intramolecular distances are detectable

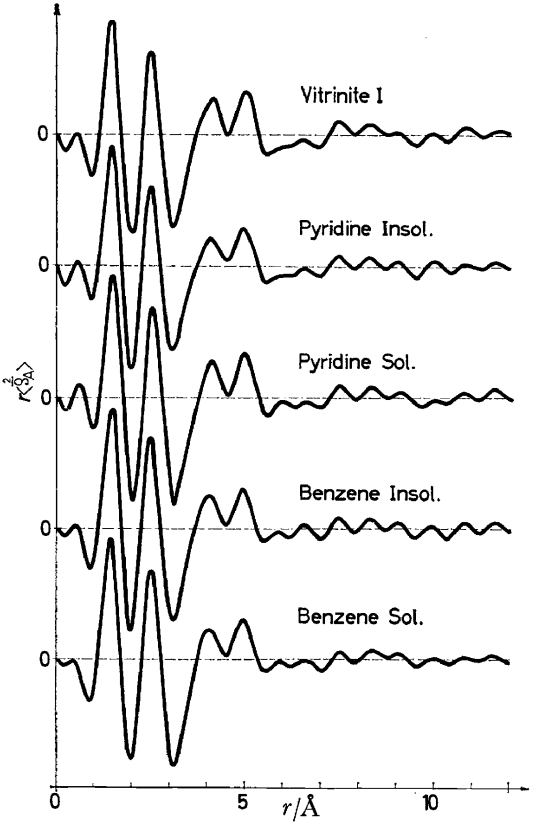

Figure 15. Radial distribution functions for the coal maceral vitrinite and various extraction products (By the courtesy of Pergamon Press).

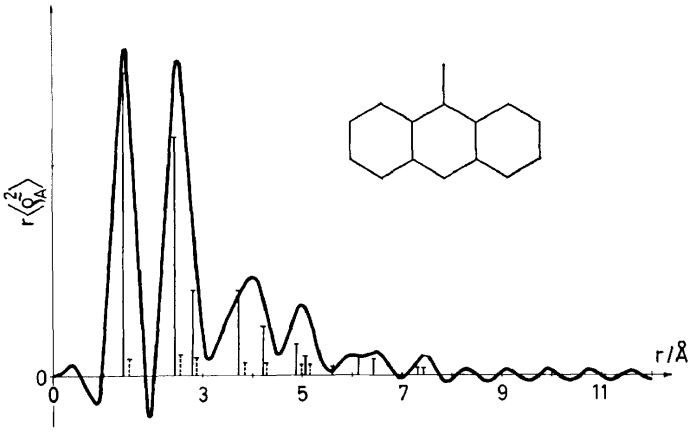

Figure 16. Theoretical radial distribution function for the carbon skeleton of 9-methylanthracene taking into account the truncation due to the upper limit in s for Cu radiation (By the courtesy of Pergamon Press).

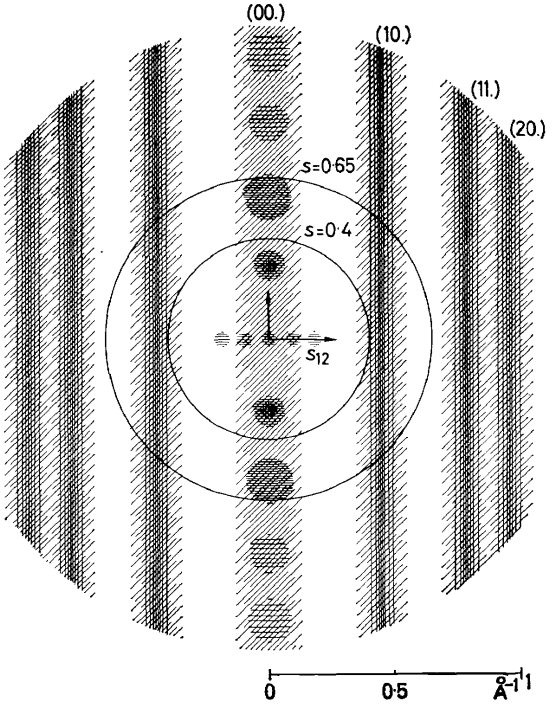

Figure 17. Theoretical intensity distribution in reciprocal space used for the evaluation of the scattering of low temperature carbonized material (By the courtesy of *Carbon*).

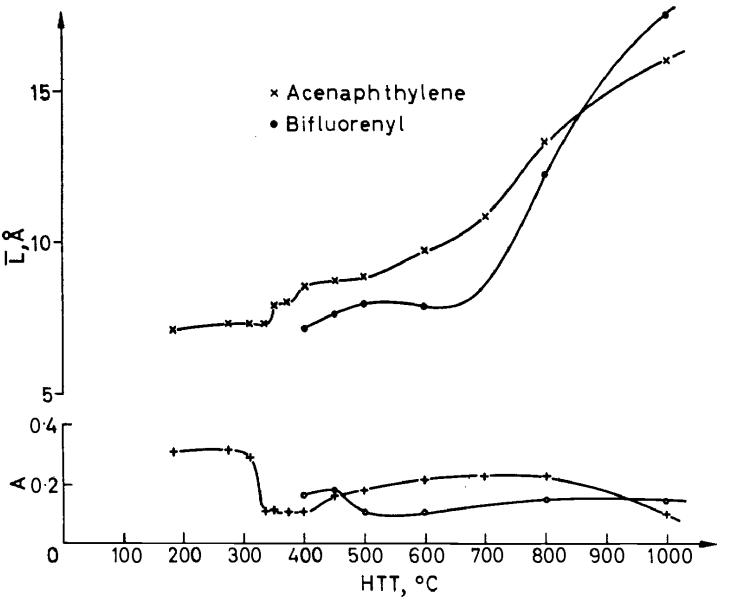

Figure 18. Molecular size $\bar{L}$ and imperfection of the hexagonal network A (By the courtesy of *Carbon*).

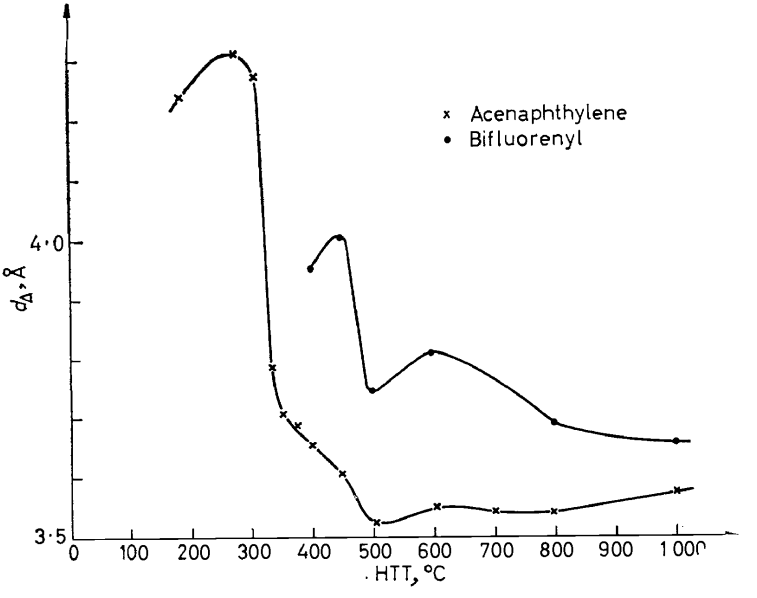

Figure 19. Average interlayer spacing (By the courtesy of *Carbon*).

up to about 7 Å, and two maxima of the intermolecular distances are present. For comparison, *Figure 16* shows the theoretical radial distribution function for the carbon skeleton of 9-methyl-anthracene calculated with the same truncation as in the experiment (Cu radiation). One can conclude from this that planar molecules with an average diameter as small as 7Å can show a definite tendency towards parallel stacking. In the present case, there are only about 2–3 together in a stack.

Figure 17 shows a scheme of the intensity distribution in reciprocal space used for the evaluation of the wide-angle and medium-angle scattering of various organic substances carbonized at low temperatures[30]. One can distinguish between three regions, the first (up to $s \simeq 0{\cdot}4$) contains essentially only intermolecular interferences, the second (between $s \simeq 0{\cdot}4$ and $s \simeq 0{\cdot}65$) shows a superposition of inter- and intramolecular interferences and in the third ($s > 0{\cdot}65$) the intermolecular interferences become negligible so that the intensity distribution is determined by intramolecular interferences only. This was found to be valid for domain sizes up to about 30 Å; for larger sizes the parallel stacking becomes more perfect and the higher order maxima of the intermolecular interferences show up more and more intensely. For sizes lower than 30 Å the scattering at s-values larger than 0·65 can thus be treated in the same way as the scattering of an entirely random distribution of molecules. Under these conditions a least square fit of suitably chosen molecular scattering curves[34, 35] can be used to obtain information on the average size and the size distribution of the molecules. *Figure 18* shows the results of such a study on the amorphous product of pyrolysis and carbonization of acenaphthalene and bifluorenyl[30], and *Figure 19* gives the interlayer spacing obtained from the intermolecular interferences. *Figure 20* shows the most probable molecular structures deduced from these studies occurring in this process. This has led to an interpretation of the possibility and the ease of graphite formation in terms of the steric features of the intermediates formed in the first steps of the pyrolysis.

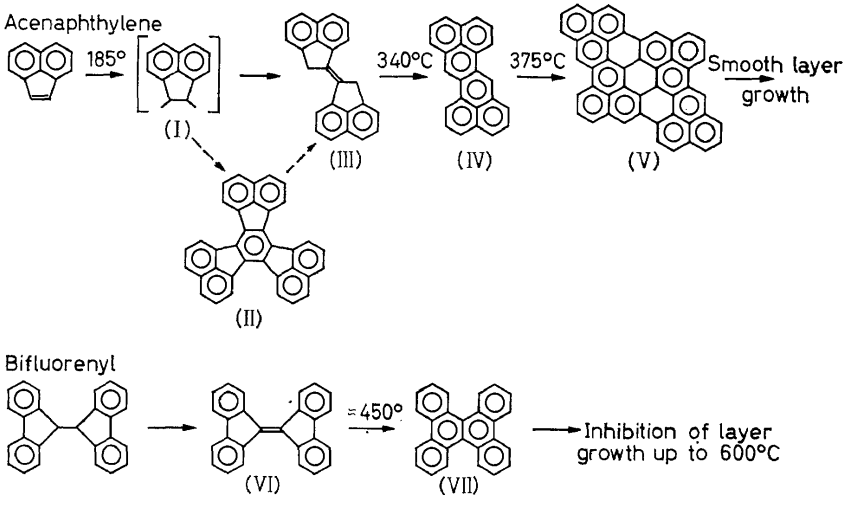

Figure 20. Initial stages of carbonization (By the courtesy of *Carbon*).

In cases of sterically unfavourable intermediates, the formation of large hexagonal layers is inhibited and one obtains an amorphous carbon which is stable up to high temperatures. Such carbons show domain sizes in the 50–100 Å range and relatively well-separated asymmetric maxima. Such maxima can be analysed by a Fourier transform method[27], and a recent study on carbons obtained from polyacrylonitrile[36] has shown the applicability of this method. *Figure 21* shows such an (hk) interference after correction for various angle-dependent factors. *Figure 22* gives the auto-correlation function

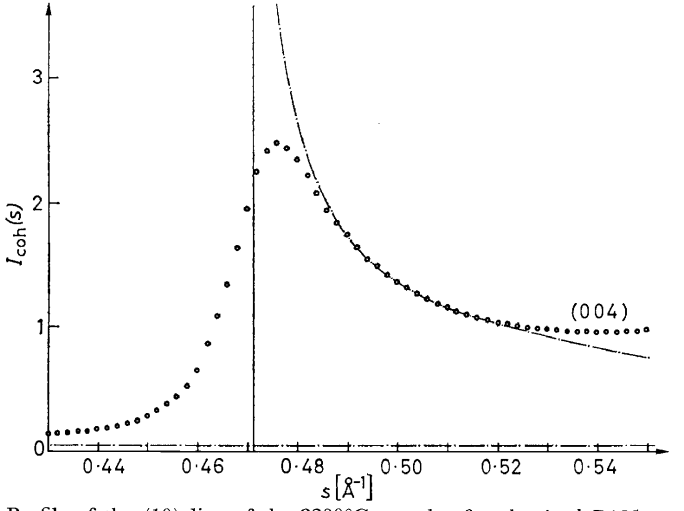

Figure 21. Profile of the (10) line of the 2200°C sample of carbonized PAN corrected for polarization, absorption, and atomic scattering, and normalized. ● — ● scattering of infinite layer

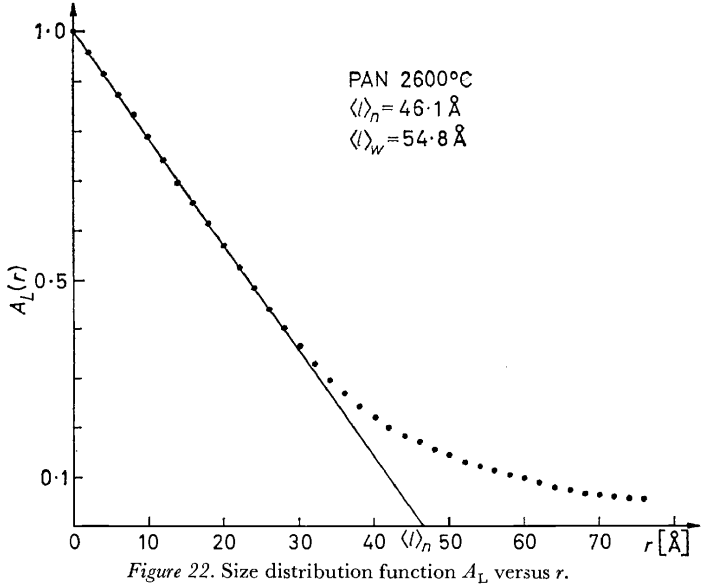

Figure 22. Size distribution function A_L versus r.

of the layer shapes obtained from the analysis of two such lines in the scattering of a polyacrylonitrile sample heated to 2600 °C in an inert atmosphere. *Figure 23* shows the mean square displacement of atoms in the layer plane relative to each other as a function of the interatomic distance and *Figure 24* the variation of the size of the layers with the temperature of heat-treatment resulting from the analysis. The conclusion drawn from this study is that the heat-treatment leads to an increase of order in the layer structure which develops from a paracrystalline state (2000 °C) over a mixed paracrystalline and strain-deformed state (2200 °C, 2400 °C) to a

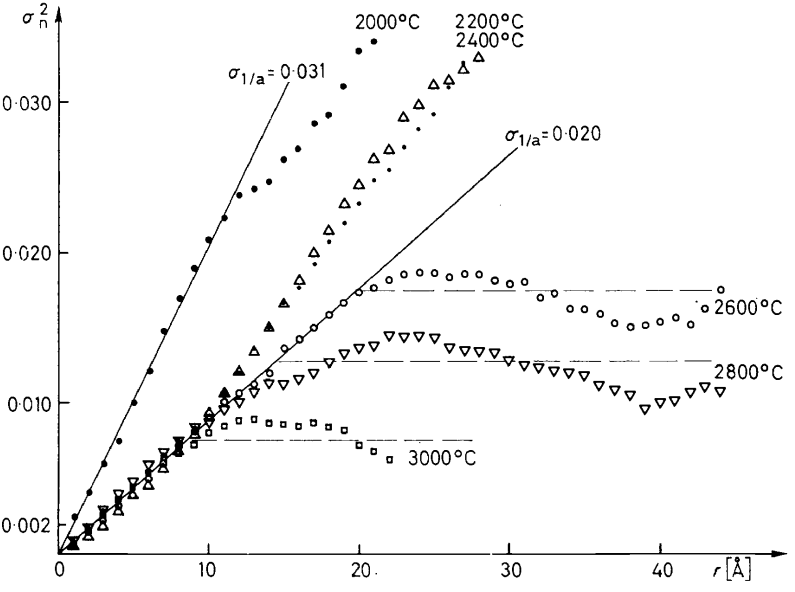

Figure 23. Variance of n-th neighbour distribution σ_n^2 - versus r.

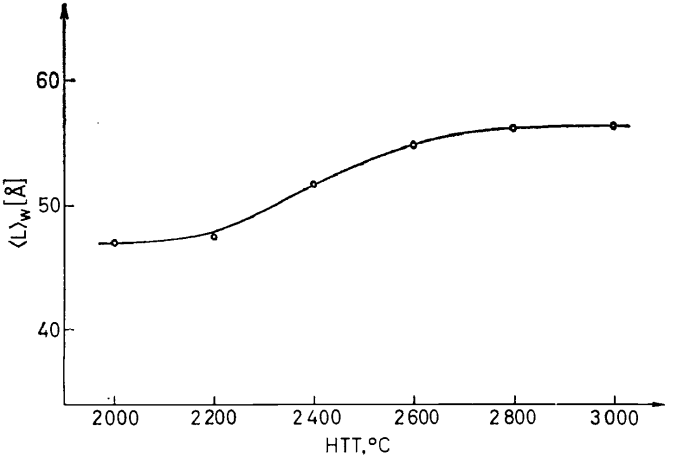

Figure 24. Weight average of $l(\langle l \rangle_w)$ versus heat treatment temperature (HTT).

structure with point defects of decreasing diameter. The layer size does not, however, increase very much (from 47 Å at 2000 °C to 57 Å at 3000 °C) and this inhibition of layer growth seems to be the important factor for the resistance against a transformation into graphite.

On the same series of samples small-angle scattering studies have been carried out[37] which show the existence of an inaccessible fine pore system with pore sizes in the 10–20 Å range. This pore system can be expected to play an important role in the inhibition of the layer growth. In the course of the small-angle studies it was found that a correct evaluation of the data is possible only if one separates the density fluctuations within the domains from the scattering of the pores. *Figure 25* shows how this separation can be obtained. A plot of $s^3\theta_{obs}$ versus s^2 (I_{obs} is the total observed small-angle

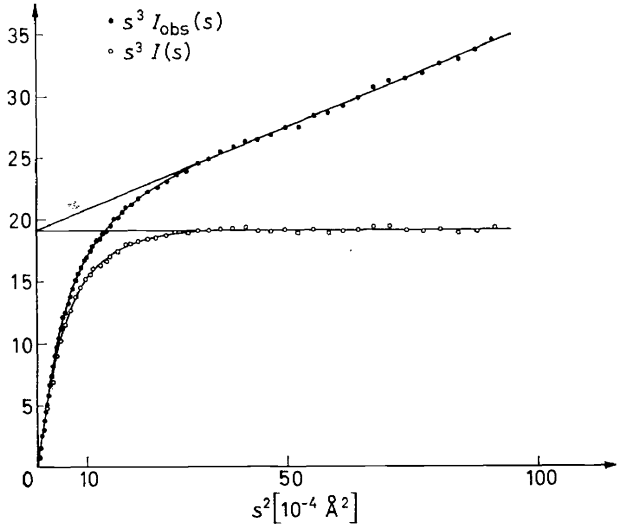

Figure 25. The function s^3I, as observed and after correction, versus s^2.

scattering measured with an infinitely high slit) reveals that there are two components of the scattering, one which shows a decrease in s^{-3} (the pore scattering following Porod's law) and another which decreases with s^{-1}. The latter stems from an anisotropic density fluctuation (perpendicular to the layer planes) in the domains due to a variation of the interlayer spacing as well as a variation of the size of the layers in a stack. In *Figure 26* the value of this fluctuation is plotted against the heat-treatment temperature. One can see that the order improves with increasing temperature. It is of interest to note that the values of the fluctuation are of the same order of magnitude as those found in liquids.

So far we have deduced the existence of the anisotropic short-range order from particular features occurring in the radial distribution functions or the radial intensity distribution. A recent electron diffraction study[38] on carbon fibres demonstrates these effects more clearly. Carbon fibres are a

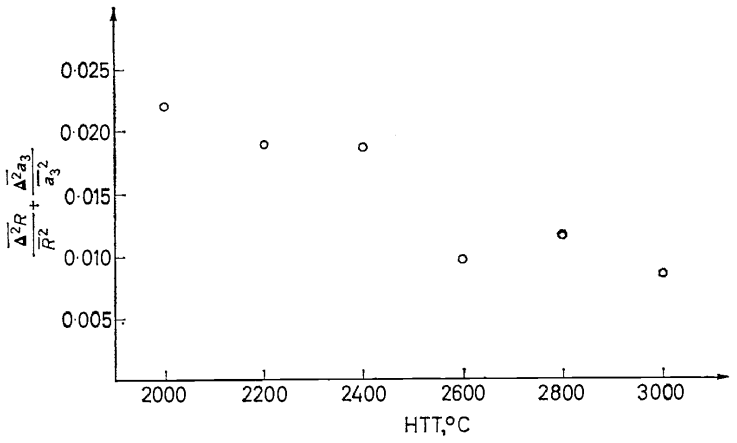

Figure 26. The variation of the density fluctuations as a function of the heat-treatment temperature for PAN carbons.

special type of amorphous carbon with about the same structure and size of the domains as other amorphous carbons but with a preferred orientation of the principal axes of the domains perpendicular to the fibre axis. *Figure 27* shows a theoretical intensity distribution of a single (*hk*) interference for such a type of preferred orientation, the primary beam is perpendicular to the fibre axis. Intensity distributions of this type can be computed for various degrees of preferred orientation using a method described by Ruland and Tompa[39]. *Figure 28* shows a schematic presentation of the effect produced by a deviation of the fibre axis from the perpendicular position. *Figures 29* and *30* show two electron diffraction diagrams, the first with the beam perpendicular to the fibre axis, the second with a slight deviation from the perpendicular position. The intra- and intermolecular interferences show up very clearly and can be separated without difficulty. The average domain size is somewhat less than 100 Å.

GENERAL CONCLUSIONS

It may be considered somewhat daring to draw general conclusions from the relatively few experimental results given in this paper. It should be emphasized, however, that these studies show the necessity for an extensive and flexible use of Fourier transform and convolution theory to interpret the scattering of amorphous materials and that the determination of a radial distribution function is by no means the end, but rather the beginning of a structural study.

As in crystal-structure determination, one should try various ways to solve the problem; sometimes the solution is easier in an appropriate interpretation of the reciprocal space, sometimes an interpretation of the auto-correlation function is more successful. If preferred orientation can be introduced, this leads generally to an increase in information.

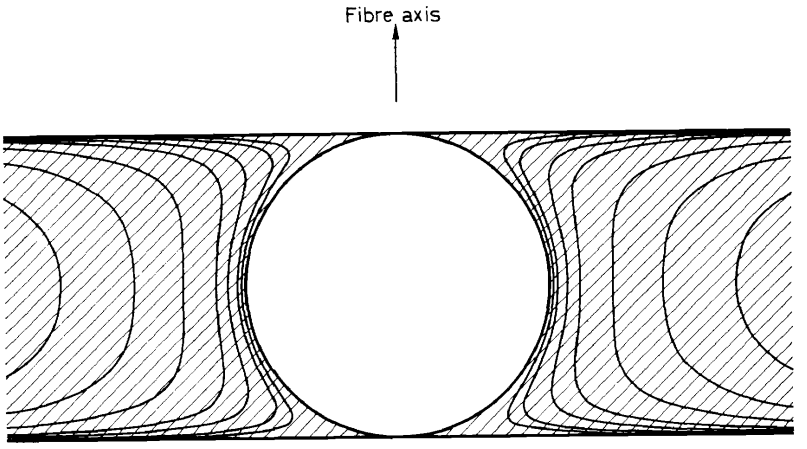

Figure 27. Theoretical intensity distribution of an (*hk*) interference for perfect orientation of the layer planes parallel to the principal axis.

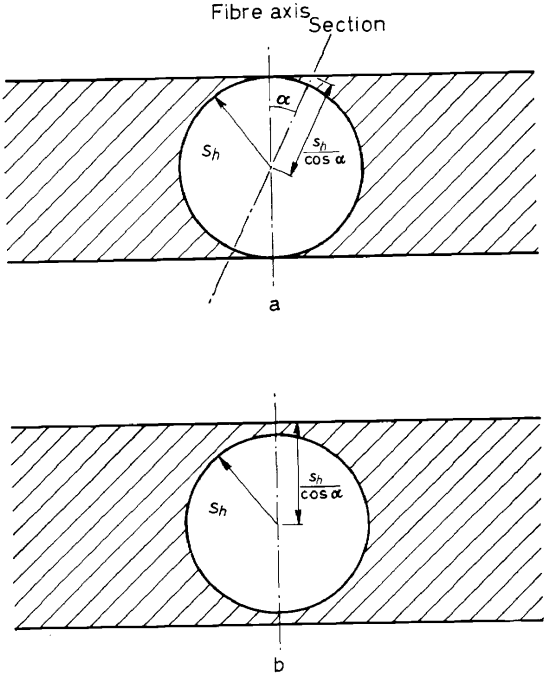

Figure 28. Schematic presentation of an oblique section through an (*hk*) interference (a) Definition of the angle α; (b) Contours of the interference function on the section.

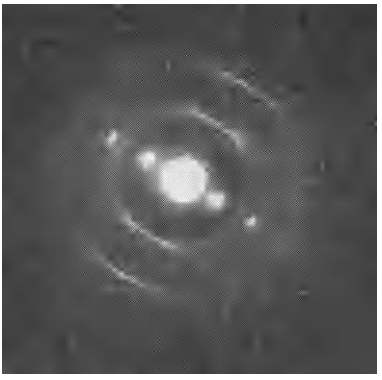

Figure 29. Electron diffraction diagram of a carbon fibre with high preferred orientation.

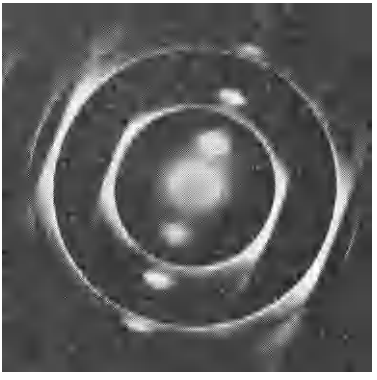

Figure 30. Electron diffraction diagram of a carbon fibre with high preferred orientation.

Our present understanding of the structure of liquids and amorphous solids is still very limited and major advances in this field are yet to come. X-ray and electron scattering together with inelastic neutron scattering will certainly play a leading role in this, especially as regards laying the foundations on which general interpretations of physical properties can be based. We may reasonably expect that science as well as technology will benefit from any progress in this field.

References

[1] W. H. Zachariasen. *J. Amer. Chem. Soc.* **34**, 3841 (1932).
[2] B. E. Warren. *J. Appl. Phys.* **8**, 645 (1937).
[3] L. R. G. Treloar. *Trans. Faraday Soc.* **39**, 36, 241 (1943).
[4] P. J. Flory. *Chem. Rev.* **35**, 51 (1944).
[5] F. T. Wall. *J. Chem. Phys.* **10**, 485 (1942).
[6] F. T. Wall. *J. Chem. Phys.* **11**, 527 (1943).
[7] J. D. Bernal. *Proc. Roy. Inst. G. Brit.* **37**, 355 (1959).

[8] R. Hosemann and S. N. Bagchi. *Direct Analysis of Diffraction by Matter*, North-Holland Publ. Co., Amsterdam (1962).
[9] R. F. Kruh. *Chem. Rev.* **62**, 319 (1962).
[10] F. Zernike and J. A. Prins. *Z. Physik* **41**, 184 (1927).
[11] J. Waser and V. Schomaker. *Rev. Mod. Phys.* **25**, 671 (1953).
[12] R. Kaplow, R. L. Strong and B. L. Averbach. *Phys. Rev.* **138**, A1336 (1965).
[13] R. R. Fessler, R. Kaplow and B. L. Averbach. *Phys. Rev.* **150**, 34 (1966).
[14] R. Kaplow, T. A. Rowe and B. L. Averbach. *Phys. Rev.* **168**, 1068 (1968).
[15] R. Hosemann and K. Lemm. *Proceedings of the International Conference of Physics of Non-Crystalline Solids*, North-Holland Publ. Co., Amsterdam, p. 85 (1964).
[16] G. W. Stewart and R. M. Morrow. *Phys. Rev.* **30**, 232 (1927).
[17] V. A. Kargin. *J. Polym. Sci.* **30**, 247 (1958).
[18] R. E. Robertson. *J. Phys. Chem.* **69**, 1575 (1965).
[19] W. Frank, H. Goddar and H. A. Stuart. *J. Polym. Sci.* **B5**, 711 (1967).
[20] G. S. Y. Yeh and P. H. Geil. *J. Macromol. Sci.* **B1**, 235 (1967).
[21] R. Bonart. *Kunstoffe* **57**, 391 (1967).
[22] R. Bonart. *Kolloid. Z. u. Z. Polymere*, in press.
[23] A. Guinier and G. Fournet. *Small-Angle Scattering of X-rays*, John Wiley & Sons, New York, p. 32 (1955).
[24] B. E. Warren. *Phys. Rev.* **59**, 693 (1941).
[25] A. J. C. Wilson. *Acta Cryst.* **2**, 245 (1949).
[26] G. W. Brindley and J. Mering. *Acta Cryst.* **4**, 441 (1951).
[27] W. Ruland. *Acta Cryst.* **22**, 615 (1967).
[28] J. R. Townsend. *Acta Cryst.* **12**, 806 (1959).
[29] B. E. Warren and P. Bodenstein. *Acta Cryst.* **18**, 282 (1965).
[30] W. Ruland. *Carbon* **2**, 365 (1965).
[31] W. Ruland. *Polymer* **5**, 89 (1964).
[32] W. Ruland. *Norelco Reporter* **14**, 12 (1967).
[33] W. Ruland. *Proceedings of the Fifth Conference on Carbon*, Pergamon Press, Vol. 1, p. 429 (1962).
[34] R. Diamond. *Acta Cryst.* **11**, 129 (1958).
[35] W. Ruland. *Acta Cryst.* **12**, 679 (1959).
[36] R. Perret and W. Ruland. *J. Appl. Cryst.* **1**, 257 (1968).
[37] R. Perret and W. Ruland. *J. Appl. Cryst.* **1**, 308 (1968).
[38] A. Fourdeux, R. Perret and W. Ruland. *J. Appl. Cryst.* **1**, 252 (1968).
[39] W. Ruland and H. Tompa. *Acta Cryst.* **A24**, 93 (1968).